Anomalous $H \to ZZ \to 4\ell$ decay and its interference effects at the LHC

Hua-Rong He[1a], Xia Wan[1b], You-Kai Wang[1c]

[1]*School of physics and Information Technology,*

Shaanxi Normal University, Xi'an 710119, China

Abstract

We calculate the spinor helicity amplitudes of anomalous $H \to ZZ \to 4\ell$ decay. After embedding these analytic formulas into the `MCFM` package, we study the interference effects between the anomalous $gg \to H \to ZZ \to 4\ell$ process and the SM processes, which are indispensable in the Higgs off-shell region. Subsequently, the constraints on the anomalous couplings are estimated using LHC experimental data.

---

[a] hehr@snnu.edu.cn

[b] wanxia@snnu.edu.cn

[c] wangyk@snnu.edu.cn

arXiv:1902.04756v2 [hep-ph] 14 Oct 2020

I. INTRODUCTION

Since the 125 GeV/c^2 Higgs boson was discovered at the Large Hadron Collider (LHC) in 2012 [1, 2], its properties have been tested more and more precisely [3–5]. Even though no new physics beyond Standard Model (SM) has been confirmed so far, it is still necessary and meaningful to search for new physics. In this paper we study the anomalous HZZ couplings.

The new physics beyond the SM in the SM effective field theory (SMEFT) is shown as higher-dimensional operators in the Lagrangian which later supply non-SM interactions. In this analysis we note these non-SM HVV (V represents Z, W, γ) interactions from six-dimensional operators as anomalous HVV couplings, and consider them separately from SM loop contributions. To scrutinize the Lorentz structures from several anomalous couplings, we calculate the scattering amplitudes in the spinor helicity method, and the analytic formulas are shown symmetrically and elegantly in the spinor notations.

HVV couplings can be probed at the LHC through processes including $V^* \to VH$ or $H \to VV$ decays. Among these processes, the $gg \to H \to ZZ \to 4\ell$ process, which is called the golden channel, is the most precise and has been studied extensively in both theoretical studies [6–41] and experiments at LHC [42–50]. Thus, we also choose this golden channel to study anomalous HVV couplings. To reach a more precise result, both on-shell and off-shell Higgs regions can be exploited. At the same time, the interference effects between this process and the SM processes should be included. Especially in the off-shell Higgs region, the interference between this process and the continuum process $gg \to ZZ \to 4\ell$ should not be ignored [51, 52]. Based on a modified `MCFM` [51, 53] package with anomalous HZZ couplings, we study the interference effects quantitatively. Furthermore, we estimate the constraints on the anomalous coupling using CMS experimental data at LHC.

The rest of the paper is organized as follows. In Section II, the spinor helicity amplitudes with anomalous couplings are calculated. In Section III, the analytic formulas are embedded into the `MCFM8.0` package and the cross sections for proton - proton collision, especially the interference effects, are shown numerically. In Section IV, the constraints on the HZZ anomalous couplings are estimated. Section V is the conclusion and discussion.

II. THEORETICAL CALCULATION

In this section firstly we introduce the HZZ anomalous couplings, and then we calculate the spinor helicity amplitudes.

A. HZZ anomalous couplings

In the SM effective field theory [54, 55] the complete form of higher-dimensional operators can be written as

$$\mathcal{L} = \mathcal{L}_{SM} + \frac{1}{\Lambda}\sum_k C_k^5 \mathcal{O}_k^5 + \frac{1}{\Lambda^2}\sum_k C_k^6 \mathcal{O}_k^6 + \mathcal{O}(\frac{1}{\Lambda^3}) \ , \tag{1}$$

where Λ is the new physics energy scale, and C_k^i with $i = 5, 6$ are Wilson loop coefficients. As the dimension-five operators $\mathcal{O}_k^5$ have no contribution to anomalous HZZ couplings, the dimension-six operators $\mathcal{O}_k^6$ have leading contributions. The relative dimension-six operators in the Warsaw basis [55] are

$$\mathcal{O}_{\Phi D}^6 = (\Phi^\dagger D^\mu \Phi)^*(\Phi^\dagger D^\mu \Phi),$$

$$\mathcal{O}_{\Phi W}^6 = \Phi^\dagger \Phi W_{\mu\nu}^I W^{I\mu\nu}, \ \ \mathcal{O}_{\Phi B}^6 = \Phi^\dagger \Phi B_{\mu\nu} B^{\mu\nu}, \ \ \mathcal{O}_{\Phi WB}^6 = \Phi^\dagger \tau^I \Phi W_{\mu\nu}^I B^{\mu\nu},$$

$$\mathcal{O}_{\Phi \tilde{W}}^6 = \Phi^\dagger \Phi \tilde{W}_{\mu\nu}^I W^{I\mu\nu}, \ \ \mathcal{O}_{\Phi \tilde{B}}^6 = \Phi^\dagger \Phi \tilde{B}_{\mu\nu} B^{\mu\nu}, \ \ \mathcal{O}_{\Phi \tilde{W} B}^6 = \Phi^\dagger \tau^I \Phi \tilde{W}_{\mu\nu}^I B^{\mu\nu}, \tag{2}$$

where Φ is a doublet representation under the $SU(2)_L$ group and the aforementioned Higgs field H is one of its four components; $D_\mu = \partial_\mu - igW_\mu^I T^I - ig'Y B_\mu$, where g and g' are coupling constants, $T^I = \tau^I/2$, where τ^I are Pauli matrices, Y is the $U(1)_Y$ generator; $W_{\mu\nu}^I = \partial_\mu W_\nu^I - \partial_\nu W_\mu^I - g\epsilon^{IJK}W_\mu^J W_\nu^K$, $B_{\mu\nu} = \partial_\mu B_\nu - \partial_\nu B_\mu$, $\tilde{W}_{\mu\nu}^I = \frac{1}{2}\epsilon_{\mu\nu\rho\sigma}W^{I\rho\sigma}$, $\tilde{B}_{\mu\nu} = \frac{1}{2}\epsilon_{\mu\nu\rho\sigma}B^{\rho\sigma}$.

For the $H \to 4\ell$ process that we are going to take to constrain the anomalous HZZ couplings numerically, there are dimension-six operators include $HZ\ell\ell$ contact interaction [56, 57] that can also contribute non-SM effects, which are

$$\mathcal{O}_{\Phi L}^6 = (\Phi^\dagger \overleftrightarrow{D}_\mu \Phi)(\bar{L}\gamma_\mu L), \ \ \mathcal{O}_{\Phi LT}^6 = (\Phi^\dagger T^I \overleftrightarrow{D}_\mu \Phi)(\bar{L}\gamma_\mu T^I L), \ \ \mathcal{O}_{\Phi e}^6 = (\Phi^\dagger \overleftrightarrow{D}_\mu \Phi)(\bar{e}\gamma_\mu e), \tag{3}$$

where $\Phi^\dagger \overleftrightarrow{D}_\mu \Phi = \Phi^\dagger D_\mu \Phi - D_\mu \Phi^\dagger \Phi$, $\Phi^\dagger T^I \overleftrightarrow{D}_\mu \Phi = \Phi^\dagger T^I D_\mu \Phi - D_\mu \Phi^\dagger T^I \Phi$, L,e represent left- and right-handed charged leptons. One may worry about the pollution caused by the $HZ\ell\ell$ contact interaction from these operators to the 4ℓ final state when probing HZZ couplings.

3

Nevertheless, we can use certain additional methods to distinguish them. In the off-shell Higgs region, the on-shell Z boson selection cut can reduce much of the $HZ\ell\ell$ background. In on-shell Higgs region, the non-leptonic Z decay channel can also be adopted in constraining HZZ couplings. These discussions are not the focus of the current paper and we are not going to examine them in detail here.

After spontaneous symmetry breaking, we get the anomalous HZZ interactions

$$\mathcal{L}_a = \frac{a_1}{v} M_Z^2 H Z^\mu Z_\mu - \frac{a_2}{v} H Z^{\mu\nu} Z_{\mu\nu} - \frac{a_3}{v} H Z^{\mu\nu} \tilde{Z}_{\mu\nu} \ , \tag{4}$$

with

$$a_1 = \frac{v^2}{\Lambda^2} C_{\Phi D}^6,$$

$$a_2 = -\frac{v^2}{\Lambda^2} (C_{\Phi W}^6 c^2 + C_{\Phi B}^6 s^2 + C_{\Phi WB}^6 cs),$$

$$a_3 = -\frac{v^2}{\Lambda^2} (C_{\Phi \tilde{W}}^6 c^2 + C_{\Phi \tilde{B}}^6 s^2 + C_{\Phi \tilde{W} B}^6 cs), \tag{5}$$

where c and s stand for the cosine and sine of the weak mixing angle respectively, a_1, a_2, a_3 are dimensionless complex numbers and $v = 246$ GeV is the electroweak vacuum expectation value. Notice that the signs before a_2 and a_3 are same as in [6, 43, 47], but have an additional minus sign from the definition in [10]. Z_μ is Z boson field, $Z_{\mu\nu} = \partial_\mu Z_\nu - \partial_\nu Z_\mu$ is the field strength tensor of the Z boson and $\tilde{Z}_{\mu\nu} = \frac{1}{2} \epsilon_{\mu\nu\rho\sigma} Z^{\rho\sigma}$ represents its dual field strength. The loop corrections in SM can contribute similarly as the a_2 and a_3 terms. Quantitatively, the one-loop correction can contribute to a_2 term with small contributions $\mathcal{O}(10^{-2} - 10^{-3})$, while the a_3 term appear in SM only at a three-loop level and thus has a even smaller contribution [43]. Therefore, only if the contributions from the a_2 and a_3 terms are larger than these loop contributions can we consider them as from new physics.

The HZZ interaction vertex from Eq. (4) is

$$\Gamma_a^{\mu\nu}(k, k') = i\frac{2}{v} \sum_{i=1}^3 a_i \Gamma_{a,i}^{\mu\nu}(k, k') = i\frac{2}{v} [a_1 M_Z^2 g^{\mu\nu} - 2a_2(k^\nu k'^\mu - k \cdot k' g^{\mu\nu}) - 2a_3 \epsilon^{\mu\nu\rho\sigma} k_\rho k'_\sigma] \ , \tag{6}$$

where k, k' are the momenta of the two Z bosons. It is worthy to notice that the HZZ vertices in the SM are

$$\Gamma_{\text{SM}}^{\mu\nu}(k, k') = i\frac{2}{v} M_Z^2 g^{\mu\nu} \ , \tag{7}$$

so the Lorentz structure of the a_1 term is same as the SM case. While the a_2 and a_3 terms have different Lorentz structures, which represent non-SM CP-even and CP-odd cases respectively.
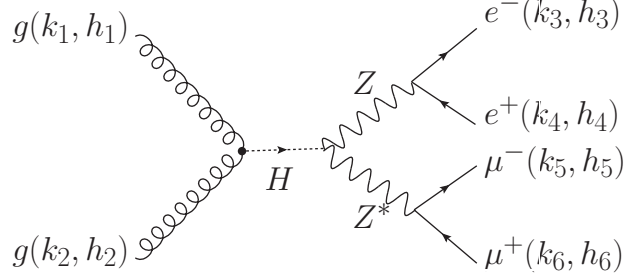
B. Helicity amplitude of the process $gg \to H \to ZZ \to 2e2\mu$

FIG. 1: Feynman diagram of the Higgs-mediated process $gg \to H \to ZZ \to 2e2\mu$. The black dot represents an effective ggH coupling from loop contributions.

The total helicity amplitude for the process $gg \to H \to ZZ \to 2e2\mu$ in Fig. 1 is composed of three individual amplitudes $A_{\rm SM}^H$, $A_{CP-\rm even}^H$ and $A_{CP-\rm odd}^H$, which have the same production process but different Higgs decay modes according to the three kinds of HZZ vertices in Eq. (6). The specific formulas are

$$\mathcal{A}^{gg \to H \to ZZ \to 2e2\mu}(1_g^{h_1}, 2_g^{h_2}, 3_{e-}^{h_3}, 4_{e+}^{h_4}, 5_{\mu-}^{h_5}, 6_{\mu+}^{h_6}) \tag{8}$$

$$= [a_1\mathcal{A}_{\rm SM}^H + a_2\mathcal{A}_{CP-\rm even}^H + a_3\mathcal{A}_{CP-\rm odd}^H](1_g^{h_1}, 2_g^{h_2}, 3_{e-}^{h_3}, 4_{e+}^{h_4}, 5_{\mu-}^{h_5}, 6_{\mu+}^{h_6}) \ , \tag{9}$$

$$= \mathcal{A}^{gg \to H}(1_g^{h_1}, 2_g^{h_2}) \times \frac{P_H(s_{12})}{s_{12}} \times \sum_{i=1}^{3} a_i \mathcal{A}_i^{H \to ZZ \to 2e2\mu}(3_{e-}^{h_3}, 4_{e+}^{h_4}, 5_{\mu-}^{h_5}, 6_{\mu+}^{h_6}) \ , \tag{10}$$

where h_i $(i = 1 \cdots 6)$ are helicity indices of external particles, $s_{ij} = (k_i + k_j)^2$ and $P_H(s) = \frac{s}{s-M_H^2+iM_H\Gamma_H}$ is the Higgs propagator.

The production part $\mathcal{A}^{gg \to H}(1_g^{h_1}, 2_g^{h_2})$ is the helicity amplitude of gluon-gluon fusion to Higgs process, in which h_1, h_2 represent the helicities of gluons with outgoing momenta. For all the other helicity amplitudes in this paper, we also keep the convention that the momentum of each external particle is outgoing. When writing the helicity amplitudes, we adopt the conventions used in [51, 58]:

$$\langle ij \rangle = \bar{u}_-(p_i)u_+(p_j), \ [ij] = \bar{u}_+(p_i)u_-(p_j) \ ,$$

$$\langle ij \rangle[ji] = 2p_i \cdot p_j, \ s_{ij} = (p_i + p_j)^2, \tag{11}$$

5

and we have

$$\mathcal{A}^{gg\to H}(1_g^+, 2_g^+) = \frac{2c_g}{v}[12]^2 \ ,$$

$$\mathcal{A}^{gg\to H}(1_g^-, 2_g^-) = \frac{2c_g}{v}\langle 12\rangle^2 \ . \tag{12}$$

To keep the ggH coupling consistent with SM, we make

$$\frac{c_g}{v} = \frac{1}{2}\sum_f \frac{\delta^{ab}}{2}\frac{i}{16\pi^2}g_s^2 4e\frac{m_f^2}{2M_W s_W}\frac{1}{s_{12}}[2 + s_{12}(1 - \tau_H)C_0^{\gamma\gamma}(m_f^2)] \ , \tag{13}$$

with

$$C_0^{\gamma\gamma}(m^2) = 2\tau_H f(\tau_H)/4m^2 \ , \tau_H = 4m^2/M_H^2, \tag{14}$$

$$f(\tau) = \begin{cases} \arcsin^2\sqrt{1/\tau} & \tau \ge 1 \\ -\frac{1}{4}\left[\log\frac{1+\sqrt{1-\tau}}{1-\sqrt{1-\tau}} - i\pi\right]^2 & \tau < 1 \end{cases} \ , \tag{15}$$

where $a, b = 1, ..., 8$ are $SU(3)_c$ adjoint representation indices for the gluons, the index f represents quark flavor and $C_0^{\gamma\gamma}(m^2)$ is the Passarino-Veltman three-point scalar function [59, 60].

The decay part $\mathcal{A}^{H\to ZZ\to 2e2\mu}(3_{e^-}^{h_3}, 4_{e^+}^{h_4}, 5_{\mu^-}^{h_5}, 6_{\mu^+}^{h_6})$ is the helicity amplitude of the process $H \to ZZ \to e^-e^+\mu^-\mu^+$, which have three sources according to the three types of vertices as written in Eq. (6). Correspondingly we write it as

$$\mathcal{A}^{H\to ZZ\to 2e2\mu}(3_{e^-}^{h_3}, 4_{e^+}^{h_4}, 5_{\mu^-}^{h_5}, 6_{\mu^+}^{h_6}) = \sum_{i=1}^3 a_i \mathcal{A}_i^{H\to ZZ\to 2e2\mu}(3_{e^-}^{h_3}, 4_{e^+}^{h_4}, 5_{\mu^-}^{h_5}, 6_{\mu^+}^{h_6}) \tag{16}$$

with

$$\mathcal{A}_1^{H\to ZZ\to 2e2\mu}(3_{e^-}^-, 4_{e^+}^+, 5_{\mu^-}^-, 6_{\mu^+}^+) = f \times l_e^2 \frac{M_W^2}{\cos^2\theta_W}\langle 35\rangle[46], \tag{17}$$

$$\mathcal{A}_2^{H\to ZZ\to 2e2\mu}(3_{e^-}^-, 4_{e^+}^+, 5_{\mu^-}^-, 6_{\mu^+}^+) = f \times l_e^2 \times$$
$$\left[2k\cdot k'\langle 35\rangle[46] + (\langle 35\rangle[45] + \langle 36\rangle[46])(\langle 35\rangle[36] + \langle 45\rangle[46])\right], \tag{18}$$

$$\mathcal{A}_3^{H\to ZZ\to 2e2\mu}(3_{e^-}^-, 4_{e^+}^+, 5_{\mu^-}^-, 6_{\mu^+}^+) = f \times l_e^2 \times (-i) \times$$
$$\left[2(k\cdot k' + \langle 46\rangle[46])\langle 35\rangle[46] + \langle 35\rangle[45](\langle 35\rangle[36] + \langle 45\rangle[46])\right.$$
$$\left. + \langle 36\rangle[46](\langle 35\rangle[36] - \langle 45\rangle[46])\right] \ . \tag{19}$$

and

$$f = -2ie^3\frac{1}{M_W\sin\theta_W}\frac{P_Z(s_{34})}{s_{34}}\frac{P_Z(s_{56})}{s_{56}} \ , \tag{20}$$

where $P_Z(s) = \frac{s}{s - M_Z^2 + iM_Z\Gamma_Z}$ is the Z boson propagator, M_Z,M_W are the masses of the Z,W bosons, θ_W is the Weinberg angle, l_e and r_e (will appear for other helicity combinations) are the coupling factors of the Z boson to left-handed and right-handed leptons:

$$l_e = \frac{-1 + 2\sin^2\theta_W}{\sin(2\theta_W)} \ , r_e = \frac{2\sin^2\theta_W}{\sin(2\theta_W)} \ . \tag{21}$$

In Eq.s (17)(18)(19), we only show the case in which the helicities of the four leptons (h_3, h_4, h_5, h_6) are equal to $(-, +, -, +)$. As for the other three non-zero helicity combinations $(-, +, +, -)$, $(+, -, -, +)$, $(+, -, +, -)$, their helicity amplitudes are similar to Eq.s (17)(18)(19), but with some exchanges such as

$$l_e \leftrightarrow r_e \ , \ 4 \leftrightarrow 6 \ , \ 3 \leftrightarrow 5 \ , \ [] \leftrightarrow \langle\rangle \ . \tag{22}$$

Their specific formulas are shown in Appendix A.

C.   Helicity amplitude of the box process $gg \to ZZ \to 2e2\mu$

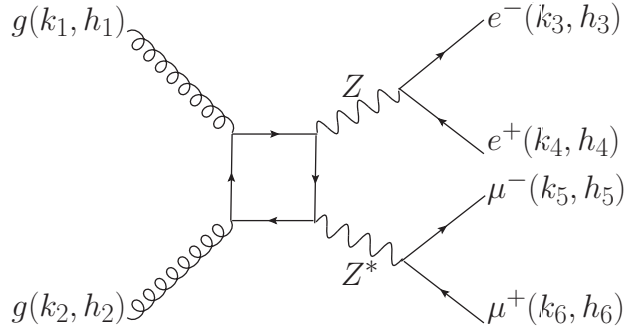FIG. 2: Feynman diagram of the box process $gg \to ZZ \to 2e2\mu$.

The box process $gg \to ZZ \to 2e2\mu$ is a continuum background of the Higgs-mediated $gg \to H \to 2e2\mu$ process. The interference between these two kinds of processes can have nonnegligible contribution in the off-shell Higgs region. The Feynman diagram of the process $gg \to ZZ \to 2e2\mu$ is a box diagram which is induced by fermion loops (see Fig. 2). The helicity amplitude $A_{\text{box}}^{gg \to ZZ \to 2e2\mu}$ has been calculated analytically and coded in MCFM8.0 package. Another similar calculation that using a different method can be found in gg2VV code [61].

D. Helicity amplitude of the process $gg \to H \to ZZ \to 4\ell$

The process $gg \to H \to ZZ \to 4\ell$ with identical $4e$ or 4μ final states can also be used to probe the anomalous HZZ couplings. In SM the differential cross sections of the 4ℓ (include both $4e$ and 4μ) and $2e2\mu$ processes are nearly the same in both on-shell and off-shell Higgs regions [53], which indicates adding the $4e/4\mu$ process can almost double experimental statistics. This situation can probably be similar for the anomalous Higgs-mediated processes. The $4e/4\mu$ Feynman diagrams consist of two different topology structures as shown in Fig. 3. Fig. 3(b) is different from Fig. 3(a) just by swapping the positive charged leptons ($4\leftrightarrow6$). The helicity amplitude of each diagram is similar to the former $2e2\mu$ cases but need to be multiplied by a symmetry factor $\frac{1}{2}$. While calculating the total cross section the interference term between Fig. 3(a) and (b) need an extra factor of -1 comparing to the self-conjugated terms because it connects all of the decayed leptons in one fermion loop while each self-conjugated term has two fermion loops. After considering these details, the summed cross section of $4e$ and 4μ processes is comparable to the $2e2\mu$ process. More details are shown in the following numerical results.
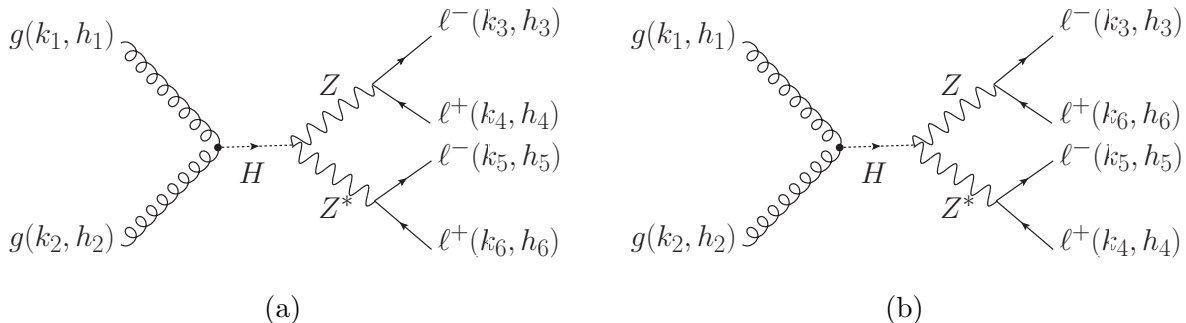

(a)   (b)

FIG. 3: The Feynman diagrams of the process $gg \to H \to ZZ \to 4\ell$, where $4\ell = 4e$ or 4μ. Note that diagram (b) is obtained by swapping the two positive charged leptons ($4\leftrightarrow6$) in diagram (a).

III. NUMERICAL RESULT

In this section we present the integrated cross sections and differential distributions in both on-shell and off-shell Higgs regions, especially the interference between anomalous Higgs-mediated processes and SM processes.

A.   The cross sections

To compare theoretical calculation with experimental observation at LHC, we need to further calculate the cross sections at hadron level. From helicity amplitude to the cross section, there need two more steps. Firstly we should sum and square the amplitudes to get the differential cross section at parton level, then integrate phase space and parton distribution function (PDF) to get the cross section at hadron level. As following we show these two steps conceptually.

The squared amplitude in the differential cross section at parton level $d\hat{\sigma}(s_{12})$ is

$$\left| \mathcal{A}_{\mathrm{box}}^{gg\to ZZ\to 4\ell} + \mathcal{A}^{gg\to H\to ZZ\to 4\ell} \right|^2 \tag{23}$$

$$= \left| \mathcal{A}_{\mathrm{box}}^{gg\to ZZ\to 4\ell} + \mathcal{A}_{\mathrm{SM}}^{H} + a_1 \mathcal{A}_{\mathrm{SM}}^{H} + a_2 \mathcal{A}_{CP-\mathrm{even}}^{H} + a_3 \mathcal{A}_{CP-\mathrm{odd}}^{H} \right|^2 . \tag{24}$$

After expanding it, there left self-conjugated terms and interference terms that have different amplitude sources. As in the next step the integral of phase space and PDF are same for each term, we note the integrated cross sections separately by the amplitude sources, which are

$$\sigma_{k,l} \sim \begin{cases} |\mathcal{A}_k|^2, & k = l; \\ 2\mathrm{Re}(\mathcal{A}_k^* \mathcal{A}_l), & k \neq l, \end{cases} \tag{25}$$

where $k, l = \{\mathrm{box},\ \mathrm{SM},\ CP\text{-even},\ CP\text{-odd}\}$. The superscripts of $\mathcal{A}$ are omitted for brevity.

B.   Numerical results for $gg \to 2e2\mu$ process

We make the integral of phase space and the PDF in the `MCFM` 8.0 package [62, 63]. The simulation is performed for the proton-proton collision at the center-of-mass energy $\sqrt{s} = 13$ TeV. The Higgs mass is set to be $M_H = 125$ GeV. The renormalization μ_r and factorization scale μ_f are set as the dynamic scale $m_{4\ell}/2$. For PDF we choose the leading-order MSTW 2008 PDFs MSTW08LO [64]. Some basic phase space cuts are exerted as follows, which are similar to the event selection cuts used in CMS experiment [65].

$$P_{T,\mu} > 5 \text{ GeV},\ |\eta_\mu| < 2.4 \ ,$$
$$P_{T,e} > 7 \text{ GeV},\ |\eta_{\mathrm{e}}| < 2.5 \ , \tag{26}$$
$$m_{\ell\ell} > 4 \text{ GeV},\ \mathrm{m}_{4\ell} > 100 \text{ GeV} \ .$$

Besides, for the $2e2\mu$ channel, the hardest (second-hardest) lepton should satisfy $P_T > 20\,(10)$ GeV; one pair of leptons with the same flavour and opposite charge is required to have 40 GeV $< \mathrm{m}_{\ell^+\ell^-} < 120$ GeV and the other pair needs to fulfill 12 GeV $< \mathrm{m}_{\ell^+\ell^-} < 120$ GeV. For the $4e$ or 4μ channel, four oppositely charge lepton pairs exist as Z boson candidates. The selection strategy is to first choose one pair nearest to the Z boson mass as one Z boson, then consider the left two leptons as the other Z boson. The other requirements are similar to the $2e2\mu$ channel.

13 TeV, $m_{2e2\mu} < 130$ GeV, on-shell				
$\sigma_{k,l}$(fb)	box	Higgs-med.		
		SM	CP-even	CP-odd
box	0.024	0	0	0
SM	0	0.503	0.558	0
CP-even	0	0.558	0.202	0
CP-odd	0	0	0	0.075

13 TeV, $m_{2e2\mu} > 220$ GeV, off-shell				
$\sigma_{k,l}$(fb)	box	Higgs-med.		
		SM	CP-even	CP-odd
box	1.283	-0.174	-0.571	0
SM	-0.174	0.100	0.137	0
CP-even	-0.571	0.137	0.720	0
CP-odd	0	0	0	0.716

TABLE I: The cross sections of $gg \to 2e2\mu$ processes in proton-proton collision at center-of-mass energy $\sqrt{s} = 13$ TeV with $a_1 = 0, a_2 = a_3 = 1$ in Eq. (6).

Table I shows the cross sections $\sigma_{k,l}$ with $k, l = \{\text{box, SM, } CP\text{-even, } CP\text{-odd}\}$ while a_1, a_2, a_3 are all set to 1 for convinience. The cross section values can be converted easily by multiplying a scale factor for small a_is. In the left and right panels, the integral regions of $m_{4\ell}$ are separately set as $m_{4\ell} < 130$ GeV and $m_{4\ell} > 220$ GeV, which correspond to the on-shell and off-shell Higgs regions, respectively. Next we focus on two kinds of interference effects: the interference between each Higgs-mediated process and box continuum background, denoted as $\sigma_{\text{box},l}$ (or $\sigma_{l,\text{box}}$) with $l \neq$ box; and the interference between different Higgs-mediated processes, denoted as $\sigma_{k,l}$ with $k, l \neq$ box.

The interference terms between Higgs-mediated processes and the continuum background $\sigma_{\text{box},l}$ are all zeros in on-shell Higgs region, but relatively sizeble in the off-shell regions except for the cases with the CP-odd Higgs-mediated process as shown in Table I. There is an

interesting reason for it. As from Eq. (9)(10)(25),

$$\sigma_{\text{box},l} \sim 2\text{Re}(\mathcal{A}_{\text{box}}^* \mathcal{A}_l) \,,$$

$$\sim 2\text{Re}\big(\mathcal{A}_{\text{box}}^* \mathcal{A}^{gg \to H} P_H(s_{12}) \mathcal{A}_i\big) \,,$$

$$\sim 2\frac{(s_{12} - M_H^2)\text{Re}\big(\mathcal{A}_{\text{box}}^* \mathcal{A}^{gg \to H} \mathcal{A}_i\big) + M_H \Gamma_H \text{Im}\big(\mathcal{A}_{\text{box}}^* \mathcal{A}^{gg \to H} \mathcal{A}_i\big)}{(s_{12} - M_H^2)^2 + M_H^2 \Gamma_H^2} \,, \qquad (27)$$

which means the integrand of $\sigma_{\text{box},l}$ consists of two parts, one is antisymmetric around M_H^2, the other is proportional to $M_H \Gamma_H \text{Im}\big(\mathcal{A}_{\text{box}}^* \mathcal{A}^{gg \to H} \mathcal{A}_i\big)$. The first part can be largely suppressed almost to zero in the integral with an integral region symmetric around M_H. The second part is also suppressed not only by the small factor of Γ_H/M_H but also by a small value of $\text{Im}\big(\mathcal{A}_{\text{box}}^* \mathcal{A}^{gg \to H} \mathcal{A}_i\big)$ in the on-shell Higgs region. By contrary, in the off-shell Higgs region the integral regions are not symmetric around M_H but in one side larger than M_H, which makes the first term have some non-zero contribution. Both the first and the second terms can also be enhanced when $\sqrt{s_{12}}$ is a little larger than twice of the top quark mass. That is because the $gg \to H$ process is induced mainly by top quark loop, both the real part and the imaginary part of the amplitude ($\text{Re}\mathcal{A}^{gg \to H}$ and $\text{Im}\mathcal{A}^{gg \to H}$) can be enhanced when $\sqrt{s_{12}}$ is just larger than the $2M_t$ threshold (see Eq. (13)). Then $\text{Im}\big(\mathcal{A}_{\text{box}}^* \mathcal{A}^{gg \to H} \mathcal{A}_i\big)$ can have a larger value, even though the relative contribution from the second term can be still suppressed by the smallness of the factor Γ_H/M_H. In conclusion, mainly due to the nonsymmetric integral region and some enhancement of $\mathcal{A}^{gg \to H}$, the interferece contribution in the off-shell Higgs region becomes comparable with the self-conjugated contributions.

It is also worthwhile to point out there is no cross section contribution from the interference between the CP-odd Higgs-mediated process and other three processes, which include the continuumm background process, SM Higgs-mediated process and anomalous CP-even Higgs-mediated process. It is because there is an antisymmetric tensor $\epsilon^{\mu\nu\rho\sigma}$ in the CP-odd HZZ interaction vertex (see last term in Eq. (6)), while in the other three processes, the two indices are symmetrically paired and so the contract of the indices makes the interference term zero. Nevertheless, these CP-odd interference term can show angular distributions, include polar angle distribution of ℓ in Z boson rest frame and azimuthal angular distribution between two z decay planes [33, 36], even though its contribution to the total cross scetion is still zero.

The interference between CP-even Higgs-mediated process and SM Higgs-mediated process is nonnegligible both in on-shell and off-shell Higgs regions. In on-shell Higgs region,

11

the contribution from interfernce terms is larger than that from the self-conjugated terms. Furthermore, for $a_1 = 0, a_2 = -1$ choice(as in [10]), the interference terms would have a minus sign, comparing to the relative values in Table I, which makes the total contribution of CP-even Higgs-mediated process beyond SM a destructive effect. In the off-shell region, the CP-even Higgs-mediated process have two interference terms, separately between SM Higgs-mediated process and the box process. These two interference terms have opposite sign, which means they cancel each other partly. Even though, the summed interfernce effect is still comparable to the self-conjugated contribution.
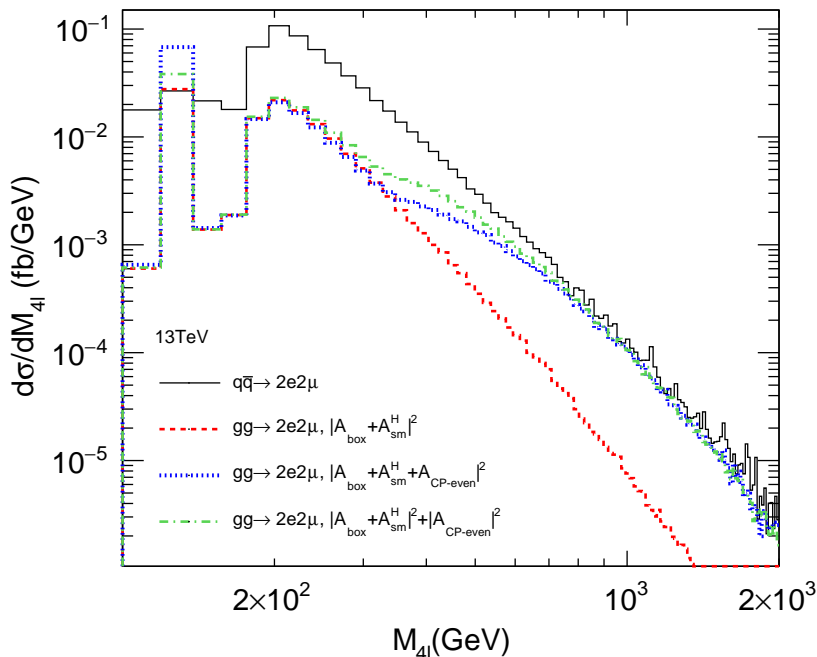

FIG. 4: Differential cross sections of the $gg \to 2e2\mu$ processes and $q\bar{q} \to 2e2\mu$ process in proton-proton collision at $\sqrt{s} = 13$ TeV with $a_2 = 1, a_1 = a_3 = 0$ in Eq. (6).

Fig. 4 shows the differential cross sections. The black histogram is from its main background process $q\bar{q} \to 2e2\mu$, which is a huge background but still controllable. The red dashed histogram is from the SM $gg \to 2e2\mu$ processes including contributions from both the box and SM Higgs-mediated amplitudes. The blue dotted histogram adds contribution from the CP-even Higgs-mediated amplitude to the SM signal and background amplitudes. Therefore three kinds of interference terms are included. For comparison, we also show the green

dashed-dotted histogram without interference terms from CP-even Higgs amplitudes with others, so the interference contribution can be calculated by the difference between blue and green histograms. In the on-shell region we can see the CP-even Higgs-mediated process have a total positive contribution (blue histogram) compare to the SM process(red histogram), while the green histogram shows the main positive contribution is from the interference term. In the off-shell region, the interference contribution is obvious in 200 GeV $<$ m$_{4\ell}$ $<$ 600 GeV region. There is a bump in blue and green histograms when $m_{4\ell} \approx 350$ GeV, which is caused by the total cross section of the CP-even Higgs-mediated process increase suddenly beyond the $2M_t$ (twice of the top quark mass) threshold. The differential cross section for the CP-odd Higgs-mediated process is similar to the green histogram in off-shell region since it has no interference contribution after the angular distributions being integrated.

The numerical results at center-of-mass energy $\sqrt{s} = 8$ TeV are shown in Table III in Appendix B. By comparing them to the results at $\sqrt{s} = 13$ TeV in Table I, we can find that each cross section is decreased by about one or two times and their relative ratios have some minor changes. That can be caused by both PDF functions and kinematic distributions.

C. Numerical results for $gg \rightarrow 4e/4\mu$ processes

13 TeV, $m_{4e/4\mu} < 130$ GeV, on-shell				
$\sigma_{k,l}$(fb)	box	Higgs-med.		
		SM	CP-even	CP-odd
box	0.045	0	0	0
SM	0	0.540	0.568	0
CP-even	0	0.568	0.186	0
CP-odd	0	0	0	0.060

13 TeV, $m_{4e/4\mu} > 220$ GeV, off-shell				
$\sigma_{k,l}$(fb)	box	Higgs-med.		
		SM	CP-even	CP-odd
box	1.303	-0.176	-0.575	0
SM	-0.176	0.101	0.137	0
CP-even	-0.575	0.137	0.740	0
CP-odd	0	0	0	0.708

TABLE II: Cross sections of $gg \rightarrow 4e/4\mu$ processes in proton-proton collisions at center-of-mass energy $\sqrt{s} = 13$ TeV with $a_1 = 0, a_2 = a_3 = 1$ in Eq. (6).

The cross sections of $gg \rightarrow 4e/4\mu$ processes are listed in Table II (Table IV in Appendix B) for comparison and next use. Here $gg \rightarrow 4e/4\mu$ represents the sum of $gg \rightarrow 4e$ and $gg \rightarrow 4\mu$. Comparing Table II with Table I, the numbers in the right panels are similar, while the

numbers in the left panels have relatively large differences. That is mainly because the different selection cuts [53]. If apply the $4e/4\mu$ selection cuts to the $gg \to 2e2\mu$ process, $\sigma_{\text{box,box}}$ in the left panels can become similar.

IV.   CONSTRAINTS: A NAIVE ESTIMATION

In this section we show a naive estimation to constrain a_1, a_2 and a_3 by using the data in both the on-shell and off-shell Higgs regions.

First, we estimate the expected number of events $N^{\text{exp}}(a_1, a_2, a_3)$ in the off-shell Higgs region, which is defined as the contribution from the processes with anomalous couplings after excluding the pure SM contributions.

A theoretical observed total number of events should be

$$N^{\text{theo}}(a_1, a_2, a_3) = \sigma_{\text{tot}} \times \mathcal{L} \times k \times \epsilon , \tag{28}$$

where σ_{tot} is the total cross section, $\mathcal{L}$ is the integrated luminosity, k represents the k-factor and ϵ is the total efficiency.

The simulation in the CMS experiment [47] with an integrated luminosity of $\mathcal{L} \sim 80$ fb^{-1} at $\sqrt{s} = 13$ TeV shows that for the $gg \to 4\ell$ process, the expected numbers of events in the off-shell Higgs region ($m_{4\ell} > 220$ GeV) can be divided into two categories: $N_{gg \text{ signal}} = 20.3$ and $N_{gg \text{ interference}} = -34.4$, where the subscript "$gg$ signal" represents the SM Higgs-mediated signal term, "gg interference" represents the interference term between SM Higgs-mediated process and the box process. For high-order corrections that may change the k-factor, some existing studies [66–69] show that the loop corrections on the box diagram (Fig.2) and the Higgs-mediated diagram are different. Therefore, we also group the expected event number contributed from the anomalous couplings into two categories.

$$
\begin{aligned}
&N^{\text{exp}}(a_1, a_2, a_3) \\
&= \frac{N_{gg \text{ signal}}}{\sigma_{\text{SM}}^H} \times [(a_1 + 1)^2 \sigma_{\text{SM}}^H - \sigma_{\text{SM}}^H + a_2^2 \sigma_{CP-\text{even}}^H + a_3^2 \sigma_{CP-\text{odd}}^H + (a_1 + 1)a_2 \sigma_{CP-\text{even,SM}}^{\text{int}}] \\
&+ \frac{N_{gg \text{ interference}}}{\sigma_{\text{SM}}^{\text{int}}} \times [a_1 \sigma_{\text{SM,box}}^{\text{int}} + a_2 \sigma_{CP-\text{even,box}}^{\text{int}}], \tag{29}
\end{aligned}
$$

where $N^{\text{exp}}(a_1, a_2, a_3)$ represents the expected number of events from anomalous CP-even and CP-odd processes, σ_k^H is the self-conjugate Higgs-mediated cross section, and $\sigma_{k,l}^{\text{int}}$ is the interference cross section with $k, l = \{\text{box, SM}, CP\text{-even}, CP\text{-odd}\}$. The first term on

the right-hand side of the equation is the contribution from the s-channel processes, and the second part is the contribution from the interference between the s-channel processes and the box diagram. For each category with the same topological Feynman diagrams, it is assumed to have the same k-factor and total efficiency ϵ, which are equal to the corresponding values for the SM process. These coefficients are extracted from experimental measurements, which are similar as the treatment in the experiments [47, 53].

The cross section of 4ℓ final states is the sum of the cross sections of $2e2\mu$, $4e$ and 4μ final states. $N^{\text{exp}}(a_1, a_2, a_3)$ can be obtained by combining the corresponding cross sections from both Table. I and Table. II.

The experimental observed number $N^{\text{obs}}(a_1, a_2, a_3)$ that corresponds to $N^{\text{exp}}(a_1, a_2, a_3)$ is defined as $N^{\text{obs}}(a_1, a_2, a_3) = N_{\text{total observed}} - N_{\text{total expected}}^{\text{SM}} = 38.7$ in the CMS experiment[47]. Its fluctuation is estimated as the $\delta_{\text{off}-\text{shell}} = \sqrt{N_{\text{total observed}}} = \sqrt{1325}$ (including both signal and background).

Second, the observed signal strength of the $gg \to H \to 4l$ process measured by CMS [70] is $\mu_{ggH}^{\text{obs}} = 0.97_{-0.09}^{+0.09}(\text{stat.})_{-0.07}^{+0.09}(\text{syst.})$. Its fluctuation is $\delta_{\text{on}-\text{shell}} = 0.127$ after a combination of both statistical and systematic errors. Theoretically, the signal strength with anomalous couplings can be estimated as

$$\mu_{ggH}^{\text{exp}}(a_1, a_2, a_3) = \frac{1}{\sigma_{\text{SM}}^H}[(a_1+1)^2\sigma_{\text{SM}}^H + a_2^2\sigma_{CP-\text{even}}^H + a_3^2\sigma_{CP-\text{odd}}^H + (a_1+1)a_2\sigma_{CP-\text{even,SM}}^{\text{int}}], \quad (30)$$

where σ_k^H and $\sigma_{k,l}^{\text{int}}$ are same as in Eq.(29) except in the on-shell region. Equation (30) is shorter than Eq.(29) because in the on-shell Higgs region the interference term with box diagram $\sigma_{\text{SM,box}}$ and $\sigma_{\text{CP}-\text{even,box}}$ are zero.

The survival parameter regions of a_1, a_2 and a_3 can be obtained by a global χ^2 fit, which can be constructed as

$$\chi^2 = \left(\frac{N^{\text{exp}} - N^{\text{obs}}}{\delta_{\text{off}-\text{shell}}}\right)^2 + \left(\frac{\mu_{ggH}^{\text{exp}} - \mu_{ggH}^{\text{obs}}}{\delta_{\text{on}-\text{shell}}}\right)^2. \quad (31)$$

The adoption of the χ^2 fit here can be controversial, as we only have two input data points (on-shell and off-shell) and have to find parameter regions for three variables (a_1, a_2 and a_3). We claim that the result here is just for a complete analysis including both theoretical calculation and experimental constraints and it is very preliminary. The situation can be improved if experimental collaborations can collect sufficient statistics in the future. Nevertheless, the χ^2 fit can also provide some interesting results.
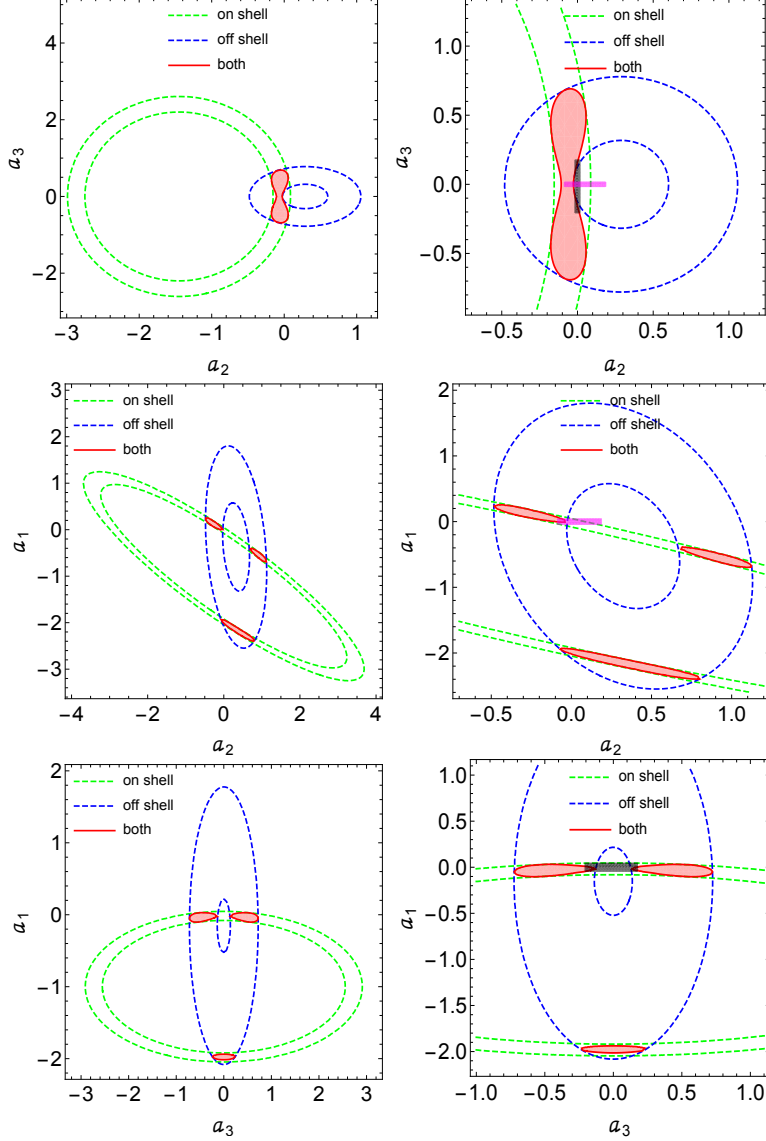
FIG. 5: Two-dimensional constraints on the new physics coefficients a_1, a_2 and a_3 from χ^2 fits. To illustrate the constraints from different energy regions, three 1σ regions (green concentric circles, blue concentric circles, and red region) from three individual χ^2 fits (on-shell, off-shell, and both) are drawn here. CMS 2σ constraints (95% confidence level) [47] are drawn as the lines (magenta for a_2 when $a_1 = a_3 = 0$ and grey for a_3 when $a_1 = a_2 = 0$) in the right zoom in plots.

Fig.5 shows the two dimensional contour diagram of the anomalous couplings. There are three colored regions (green, blue, and red) in each small plot and the red areas are the final 1σ survival parameter regions from the global χ^2 fit. In the actual two dimensional fitting procedure, we take two anomalous couplings to be free and fix the third one to be

16

zero. Three individual χ^2 fits are operated, constraint only from the off-region (first part in Eq. (31)), constraint from the on-shell region (second part in Eq. (31)) and both of the two. The purpose is to show how the irregular overlap red regions come from. As discussed in above sections, we have equal number of experimental data points and free parameters here and the χ^2 fit degenerates to an equation solving problem. Survival parameter regions from either on-shell or off-shell constraint come to be concentric circles and the global fitting results are almost the overlap region between them.

In the recently updated CMS experiment [47], it use both on-shell and off-shell data, construct kinematic discriminants, and get the limit (at 95% confidence level) of the parameters $a_2 \subset [-0.09, 0.19]$, $a_3 \subset [-0.21, 0.18]$ (there is no corresponding constraint on a_1). This experimental analysis is based on one free parameter-fitting schedule so we draw them as the line segments in the right plots of Fig. 5 (magenta for a_2 and grey for a_3). Our global fit results is roughly consistent with the CMS's, although within a first glance the two seems have some tension(Pay attention that we draw 1σ contour while CMS's results are the limit at 95% confidence level which corresponds to 2σ intervals in the hypothesis of Gaussian distribution). The CMS's results seems to be more stringent than ours. This maybe caused by more kinematic information in detail they used in their analysis. Besides, we have some parameter regions with $a_1 \sim -2$ or a_2 approaching 1. These regions show the correlations of each pairs of parameters. There is cancellation on the cross sections when the parameters coexist. In principle, the anomalous couplings should be much smaller than 1 to validate the operator expansion. Therefore, these parameter regions should be ruled out. Nevertheless, our global fit provides a complementary perspective of how the final anomalous coupling parameters contour regions are obtained from the individual on-shell/off-shell energy region constraints. These preliminary fitting results can be optimized in the case of more statistics in the future.

V. CONCLUSION AND DISCUSSION

When considering the anomalous HZZ couplings, we calculate the cross sections induced by these new couplings, and special attention is focused on the interference effects. In principle, there are three kinds of interference: 1. the interference between anomalous CP-even Higgs-mediated process and the continuum background box process $\sigma_{CP\text{-even,box}}$; 2. the

interference between anomalous CP-even Higgs-mediated process and SM Higgs-mediated process $\sigma_{CP\text{-even,SM}}$; and 3. the interference between the anomalous CP-odd Higgs-mediated process and all other processes $\sigma_{CP\text{-odd},k}$ with $k = \text{box, SM}, CP$-even. The numerical results of the integrated cross sections show that the first kind of interference can be neglected in the on-shell Higgs region but is nonnegligible in the off-shell Higgs region, the second kind of interference is important in both the on-shell and off-shell Higgs regions, and the third kind of interference has zero contribution for the total cross section in both regions.

By using the theoretical calculation together with both on-shell and off-shell Higgs experimental data, we estimate the constraints on the anomalous HZZ couplings. The correlations of the different kinds of anomalous couplings are shown in contour plots, which illustrate how the anomalous contributions cancel each other out and the extra parameter regions survive when they coexist.

In this research we only use the numerical results of integrated cross sections, whereas in fact more information can be fetched from the differential cross sections (kinematic distributions). Furthermore, the k-factors and total efficiencies should also be estimated separately according to different sources. We leave them for our future work.

Appendix A: Helicity amplitudes for the process $H \to ZZ \to e^- e^+ \mu^- \mu^+$

The helicity amplitudes $\mathcal{A}_1$, $\mathcal{A}_2$ and $\mathcal{A}_3$ are shown separately. The common factor f is defined as

$$f = -2ie^3 \frac{1}{M_W \sin\theta_W} \frac{P_Z(s_{34})}{s_{34}} \frac{P_Z(s_{56})}{s_{56}} \ .$$

$$\mathcal{A}_1^{H\to ZZ\to 2e2\mu}(3_{e^-}^-,4_{e^+}^+,5_{\mu^-}^-,6_{\mu^+}^+) = f \times l_e^2 \frac{M_W^2}{\cos^2\theta_W}\langle 35\rangle[46],$$

$$\mathcal{A}_1^{H\to ZZ\to 2e2\mu}(3_{e^-}^-,4_{e^+}^+,5_{\mu^-}^+,6_{\mu^+}^+) = f \times l_e r_e \frac{M_W^2}{\cos^2\theta_W}\langle 36\rangle[45],$$

$$\mathcal{A}_1^{H\to ZZ\to 2e2\mu}(3_{e^-}^+,4_{e^+}^-,5_{\mu^-}^-,6_{\mu^+}^+) = f \times l_e r_e \frac{M_W^2}{\cos^2\theta_W}\langle 45\rangle[36],$$

$$\mathcal{A}_1^{H\to ZZ\to 2e2\mu}(3_{e^-}^+,4_{e^+}^-,5_{\mu^-}^+,6_{\mu^+}^-) = f \times r_e^2 \frac{M_W^2}{\cos^2\theta_W}\langle 46\rangle[35] \ . \tag{A1}$$

$$\mathcal{A}_2^{H\to ZZ\to 2e2\mu}(3_{e^-}^-,4_{e^+}^+,5_{\mu^-}^-,6_{\mu^+}^+) = f \times l_e^2 \times$$
$$\left[2k\cdot k'\langle 35\rangle[46] + \big(\langle 35\rangle[45] + \langle 36\rangle[46]\big)\big(\langle 35\rangle[36] + \langle 45\rangle[46]\big)\right],$$

$$\mathcal{A}_2^{H\to ZZ\to 2e2\mu}(3_{e^-}^-,4_{e^+}^+,5_{\mu^-}^+,6_{\mu^+}^-) = f \times l_e r_e \times$$
$$\left[2k\cdot k'\langle 36\rangle[45] + \big(\langle 35\rangle[45] + \langle 36\rangle[46]\big)\big(\langle 36\rangle[35] + \langle 46\rangle[45]\big)\right],$$

$$\mathcal{A}_2^{H\to ZZ\to 2e2\mu}(3_{e^-}^+,4_{e^+}^-,5_{\mu^-}^-,6_{\mu^+}^+) = f \times r_e l_e \times$$
$$\left[2k\cdot k'\langle 45\rangle[36] + \big(\langle 45\rangle[35] + \langle 46\rangle[36]\big)\big(\langle 35\rangle[36] + \langle 45\rangle[46]\big)\right],$$

$$\mathcal{A}_2^{H\to ZZ\to 2e2\mu}(3_{e^-}^+,4_{e^+}^-,5_{\mu^-}^+,6_{\mu^+}^-) = f \times r_e^2 \times$$
$$\left[2k\cdot k'\langle 46\rangle[35] + \big(\langle 45\rangle[35] + \langle 46\rangle[36]\big)\big(\langle 36\rangle[35] + \langle 46\rangle[45]\big)\right]. \tag{A2}$$

$$\mathcal{A}_3^{H\to ZZ\to 2e2\mu}(3_{e^-}^-,4_{e^+}^+,5_{\mu^-}^-,6_{\mu^+}^+) = f \times l_e^2 \times (-i)\times$$
$$\left[2\big(k\cdot k' + \langle 46\rangle[46]\big)\langle 35\rangle[46] + \langle 35\rangle[45]\big(\langle 35\rangle[36] + \langle 45\rangle[46]\big)\right.$$
$$\left. + \langle 36\rangle[46]\big(\langle 35\rangle[36] - \langle 45\rangle[46]\big)\right] \ ,$$

$$\mathcal{A}_3^{H\to ZZ\to 2e2\mu}(3_{e^-}^-,4_{e^+}^+,5_{\mu^-}^+,6_{\mu^+}^-) = f \times l_e r_e \times (-i)\times$$
$$\left[2\big(k\cdot k' + \langle 45\rangle[45]\big)\langle 36\rangle[45] + \langle 36\rangle[46]\big(\langle 36\rangle[35] + \langle 46\rangle[45]\big)\right.$$
$$\left. + \langle 35\rangle[45]\big(\langle 36\rangle[35] - \langle 46\rangle[45]\big)\right],$$

$$\mathcal{A}_3^{H\to ZZ\to 2e2\mu}(3_{e^-}^+,4_{e^+}^-,5_{\mu^-}^-,6_{\mu^+}^+) = f \times r_e l_e \times (-i)\times$$
$$\left[2\big(k\cdot k' + \langle 36\rangle[36]\big)\langle 45\rangle[36] + \langle 45\rangle[35]\big(\langle 45\rangle[46] + \langle 35\rangle[36]\big)\right.$$
$$\left. + \langle 46\rangle[36]\big(\langle 45\rangle[46] - \langle 35\rangle[36]\big)\right],$$

$$\mathcal{A}_3^{H\to ZZ\to 2e2\mu}(3_{e^-}^+,4_{e^+}^-,5_{\mu^-}^+,6_{\mu^+}^-) = f \times r_e^2 \times (-i)\times$$
$$\left[2\big(k\cdot k' + \langle 35\rangle[35]\big)\langle 46\rangle[35] + \langle 46\rangle[36]\big(\langle 46\rangle[45] + \langle 36\rangle[35]\big)\right.$$
$$\left. + \langle 45\rangle[35]\big(\langle 46\rangle[45] - \langle 36\rangle[35]\big)\right]. \tag{A3}$$

19

Appendix B: The cross sections at $\sqrt{s} = 8$ TeV

8 TeV, $m_{2e2\mu} < 130$ GeV, on-shell				
$\sigma_{k,l}$(fb)	box	Higgs-med.		
		SM	CP-even	CP-odd
box	0.011	0	0	0
SM	0	0.232	0.257	0
CP-even	0	0.257	0.093	0
CP-odd	0	0	0	0.035

8 TeV, $m_{2e2\mu} > 220$ GeV, off-shell				
$\sigma_{k,l}$(fb)	box	Higgs-med.		
		SM	CP-even	CP-odd
box	0.479	-0.056	-0.198	0
SM	-0.056	0.031	0.047	0
CP-even	-0.198	0.047	0.228	0
CP-odd	0	0	0	0.219

TABLE III: Cross sections of $gg \to 2e2\mu$ process in proton-proton collision at $\sqrt{s} = 8$ TeV with $a_1 = 0, a_2 = a_3 = 1$ in Eq. (6).

8 TeV, $m_{4e/4\mu} < 130$ GeV, on-shell				
$\sigma_{k,l}$(fb)	box	Higgs-med.		
		SM	CP-even	CP-odd
box	0.021	0	0	0
SM	0	0.248	0.261	0
CP-even	0	0.261	0.086	0
CP-odd	0	0	0	0.028

8 TeV, $m_{4e/4\mu} > 220$ GeV, off-shell				
$\sigma_{k,l}$(fb)	box	Higgs-med.		
		SM	CP-even	CP-odd
box	0.485	-0.056	-0.199	0
SM	-0.056	0.031	0.047	0
CP-even	-0.199	0.047	0.229	0
CP-odd	0	0	0	0.215

TABLE IV: The cross sections of $gg \to 4e/4\mu$ processes in proton-proton collision at center-of-mass energy $\sqrt{s} = 8$ TeV with $a_1 = 0, a_2 = a_3 = 1$ in Eq. (6).

[1] **CMS** Collaboration, S. Chatrchyan *et al.*, "Observation of a new boson at a mass of 125 GeV with the CMS experiment at the LHC," *Phys. Lett.* **B716** (2012) 30–61, arXiv:1207.7235 [hep-ex].

[2] **ATLAS** Collaboration, G. Aad *et al.*, "Observation of a new particle in the search for the Standard Model Higgs boson with the ATLAS detector at the LHC," *Phys. Lett.* **B716** (2012) 1–29, arXiv:1207.7214 [hep-ex].

[3] **CMS** Collaboration, A. M. Sirunyan *et al.*, "Combined measurements of Higgs boson couplings in proton-proton collisions at $\sqrt{s} = 13$ TeV," *Submitted to: Eur. Phys. J.* (2018) , `arXiv:1809.10733 [hep-ex]`.

[4] **CMS** Collaboration, J. Tao, "Measurements of the 125 GeV Higgs boson at CMS," in *21st High-Energy Physics International Conference in Quantum Chromodynamics (QCD 18) Montpellier, France, July 2-6, 2018.* 2018. `arXiv:1810.00256 [hep-ex]`.

[5] **ATLAS, CMS** Collaboration, A.-M. Magnan, "The Higgs boson at the LHC: standard model Higgs properties and beyond standard model searches," *PoS* **ALPS2018** (2018) 013.

[6] Y. Gao, A. V. Gritsan, Z. Guo, K. Melnikov, M. Schulze, and N. V. Tran, "Spin determination of single-produced resonances at hadron colliders," *Phys. Rev.* **D81** (2010) 075022, `arXiv:1001.3396 [hep-ph]`.

[7] S. Bolognesi, Y. Gao, A. V. Gritsan, K. Melnikov, M. Schulze, N. V. Tran, and A. Whitbeck, "On the spin and parity of a single-produced resonance at the LHC," *Phys. Rev.* **D86** (2012) 095031, `arXiv:1208.4018 [hep-ph]`.

[8] I. Anderson *et al.*, "Constraining anomalous HVV interactions at proton and lepton colliders," *Phys. Rev.* **D89** (2014) no. 3, 035007, `arXiv:1309.4819 [hep-ph]`.

[9] Y. Chen, N. Tran, and R. Vega-Morales, "Scrutinizing the Higgs Signal and Background in the $2e2\mu$ Golden Channel," *JHEP* **01** (2013) 182, `arXiv:1211.1959 [hep-ph]`.

[10] Y. Chen and R. Vega-Morales, "Extracting Effective Higgs Couplings in the Golden Channel," *JHEP* **04** (2014) 057, `arXiv:1310.2893 [hep-ph]`.

[11] Y. Chen, E. Di Marco, J. Lykken, M. Spiropulu, R. Vega-Morales, and S. Xie, "8D likelihood effective Higgs couplings extraction framework in $h \to 4\ell$," *JHEP* **01** (2015) 125, `arXiv:1401.2077 [hep-ex]`.

[12] Y. Chen, E. Di Marco, J. Lykken, M. Spiropulu, R. Vega-Morales, and S. Xie, "Technical Note for 8D Likelihood Effective Higgs Couplings Extraction Framework in the Golden Channel," `arXiv:1410.4817 [hep-ph]`.

[13] C. A. Nelson, "Correlation Between Decay Planes in Higgs Boson Decays Into W Pair (Into Z Pair)," *Phys. Rev.* **D37** (1988) 1220.

[14] A. Soni and R. M. Xu, "Probing CP violation via Higgs decays to four leptons," *Phys. Rev.* **D48** (1993) 5259–5263, `arXiv:hep-ph/9301225 [hep-ph]`.

[15] D. Chang, W.-Y. Keung, and I. Phillips, "CP odd correlation in the decay of neutral Higgs

boson into Z Z, W+ W-, or t anti-t," *Phys. Rev.* **D48** (1993) 3225–3234, `arXiv:hep-ph/9303226 [hep-ph]`.

[16] T. Arens and L. M. Sehgal, "Energy spectra and energy correlations in the decay H → Z Z → mu+ mu- mu+ mu-," *Z. Phys.* **C66** (1995) 89–94, `arXiv:hep-ph/9409396 [hep-ph]`.

[17] S. Y. Choi, D. J. Miller, M. M. Muhlleitner, and P. M. Zerwas, "Identifying the Higgs spin and parity in decays to Z pairs," *Phys. Lett.* **B553** (2003) 61–71, `arXiv:hep-ph/0210077 [hep-ph]`.

[18] C. P. Buszello, I. Fleck, P. Marquard, and J. J. van der Bij, "Prospective analysis of spin- and CP-sensitive variables in H→Z Z → l(1)+ l(1)- l(2)+ l(2)- at the LHC," *Eur. Phys. J.* **C32** (2004) 209–219, `arXiv:hep-ph/0212396 [hep-ph]`.

[19] R. M. Godbole, D. J. Miller, and M. M. Muhlleitner, "Aspects of CP violation in the H ZZ coupling at the LHC," *JHEP* **12** (2007) 031, `arXiv:0708.0458 [hep-ph]`.

[20] V. A. Kovalchuk, "Model-independent analysis of CP violation effects in decays of the Higgs boson into a pair of the W and Z bosons," *J. Exp. Theor. Phys.* **107** (2008) 774–786.

[21] Q.-H. Cao, C. B. Jackson, W.-Y. Keung, I. Low, and J. Shu, "The Higgs Mechanism and Loop-induced Decays of a Scalar into Two Z Bosons," *Phys. Rev.* **D81** (2010) 015010, `arXiv:0911.3398 [hep-ph]`.

[22] A. De Rujula, J. Lykken, M. Pierini, C. Rogan, and M. Spiropulu, "Higgs look-alikes at the LHC," *Phys. Rev.* **D82** (2010) 013003, `arXiv:1001.5300 [hep-ph]`.

[23] J. S. Gainer, K. Kumar, I. Low, and R. Vega-Morales, "Improving the sensitivity of Higgs boson searches in the golden channel," *JHEP* **11** (2011) 027, `arXiv:1108.2274 [hep-ph]`.

[24] B. Coleppa, K. Kumar, and H. E. Logan, "Can the 126 GeV boson be a pseudoscalar?," *Phys. Rev.* **D86** (2012) 075022, `arXiv:1208.2692 [hep-ph]`.

[25] D. Stolarski and R. Vega-Morales, "Directly Measuring the Tensor Structure of the Scalar Coupling to Gauge Bosons," *Phys. Rev.* **D86** (2012) 117504, `arXiv:1208.4840 [hep-ph]`.

[26] R. Boughezal, T. J. LeCompte, and F. Petriello, "Single-variable asymmetries for measuring the 'Higgs' boson spin and CP properties," `arXiv:1208.4311 [hep-ph]`.

[27] P. Avery *et al.*, "Precision studies of the Higgs boson decay channel $H \to ZZ \to 4\ell$ with MEKD," *Phys. Rev.* **D87** (2013) no. 5, 055006, `arXiv:1210.0896 [hep-ph]`.

[28] J. M. Campbell, W. T. Giele, and C. Williams, "Extending the Matrix Element Method to Next-to-Leading Order," in *Proceedings, 47th Rencontres de Moriond on QCD and High*

Energy Interactions: La Thuile, France, March 10-17, 2012, pp. 319–322. 2012.
`arXiv:1205.3434 [hep-ph]`.

`http://lss.fnal.gov/archive/2012/conf/fermilab-conf-12-176-t.pdf`.

[29] J. M. Campbell, W. T. Giele, and C. Williams, "The Matrix Element Method at Next-to-Leading Order," *JHEP* **11** (2012) 043, `arXiv:1204.4424 [hep-ph]`.

[30] A. Menon, T. Modak, D. Sahoo, R. Sinha, and H.-Y. Cheng, "Inferring the nature of the boson at 125-126 GeV," *Phys. Rev.* **D89** (2014) no. 9, 095021, `arXiv:1301.5404 [hep-ph]`.

[31] Y. Sun, X.-F. Wang, and D.-N. Gao, "CP mixed property of the Higgs-like particle in the decay channel $h \to ZZ^* \to 4l$," *Int. J. Mod. Phys.* **A29** (2014) 1450086, `arXiv:1309.4171 [hep-ph]`.

[32] J. S. Gainer, J. Lykken, K. T. Matchev, S. Mrenna, and M. Park, "Geolocating the Higgs Boson Candidate at the LHC," *Phys. Rev. Lett.* **111** (2013) 041801, `arXiv:1304.4936 [hep-ph]`.

[33] G. Buchalla, O. Cata, and G. D'Ambrosio, "Nonstandard Higgs couplings from angular distributions in $h \to Z\ell^+\ell^-$," *Eur. Phys. J.* **C74** (2014) no. 3, 2798, `arXiv:1310.2574 [hep-ph]`.

[34] M. Chen, T. Cheng, J. S. Gainer, A. Korytov, K. T. Matchev, P. Milenovic, G. Mitselmakher, M. Park, A. Rinkevicius, and M. Snowball, "The role of interference in unraveling the ZZ-couplings of the newly discovered boson at the LHC," *Phys. Rev.* **D89** (2014) no. 3, 034002, `arXiv:1310.1397 [hep-ph]`.

[35] N. Kauer and G. Passarino, "Inadequacy of zero-width approximation for a light Higgs boson signal," *JHEP* **08** (2012) 116, `arXiv:1206.4803 [hep-ph]`.

[36] M. Beneke, D. Boito, and Y.-M. Wang, "Anomalous Higgs couplings in angular asymmetries of $H \to Z\ell^+\ell^-$ and e$^+$ e$^- \to HZ$," *JHEP* **11** (2014) 028, `arXiv:1406.1361 [hep-ph]`.

[37] A. Falkowski and R. Vega-Morales, "Exotic Higgs decays in the golden channel," *JHEP* **12** (2014) 037, `arXiv:1405.1095 [hep-ph]`.

[38] T. Modak, D. Sahoo, R. Sinha, H.-Y. Cheng, and T.-C. Yuan, "Disentangling the Spin-Parity of a Resonance via the Gold-Plated Decay Mode," *Chin. Phys.* **C40** (2016) no. 3, 033002, `arXiv:1408.5665 [hep-ph]`.

[39] M. Gonzalez-Alonso and G. Isidori, "The $h \to 4l$ spectrum at low m_{34}: Standard Model vs. light New Physics," *Phys. Lett.* **B733** (2014) 359–365, `arXiv:1403.2648 [hep-ph]`.

[40] N. Belyaev, R. Konoplich, L. E. Pedersen, and K. Prokofiev, "Angular asymmetries as a probe for anomalous contributions to HZZ vertex at the LHC," *Phys. Rev.* **D91** (2015) no. 11, 115014, `arXiv:1502.03045 [hep-ph]`.

[41] J. S. Gainer *et al.*, "Adding pseudo-observables to the four-lepton experimentalist's toolbox," *JHEP* **10** (2018) 073, `arXiv:1808.00965 [hep-ph]`.

[42] **CMS** Collaboration, S. Chatrchyan *et al.*, "Study of the Mass and Spin-Parity of the Higgs Boson Candidate Via Its Decays to Z Boson Pairs," *Phys. Rev. Lett.* **110** (2013) no. 8, 081803, `arXiv:1212.6639 [hep-ex]`.

[43] **CMS** Collaboration, V. Khachatryan *et al.*, "Constraints on the spin-parity and anomalous HVV couplings of the Higgs boson in proton collisions at 7 and 8 TeV," *Phys. Rev.* **D92** (2015) no. 1, 012004, `arXiv:1411.3441 [hep-ex]`.

[44] **CMS** Collaboration, V. Khachatryan *et al.*, "Constraints on the Higgs boson width from off-shell production and decay to Z-boson pairs," *Phys. Lett.* **B736** (2014) 64–85, `arXiv:1405.3455 [hep-ex]`.

[45] **LHC Higgs Cross Section Working Group** Collaboration, D. de Florian *et al.*, "Handbook of LHC Higgs Cross Sections: 4. Deciphering the Nature of the Higgs Sector," `arXiv:1610.07922 [hep-ph]`.

[46] **CMS** Collaboration, A. M. Sirunyan *et al.*, "Constraints on anomalous Higgs boson couplings using production and decay information in the four-lepton final state," *Phys. Lett.* **B775** (2017) 1–24, `arXiv:1707.00541 [hep-ex]`.

[47] **CMS** Collaboration, A. M. Sirunyan *et al.*, "Measurements of the Higgs boson width and anomalous HVV couplings from on-shell and off-shell production in the four-lepton final state," *Phys. Rev. D* **99** (2019) no. 11, 112003, `arXiv:1901.00174 [hep-ex]`.

[48] **ATLAS** Collaboration, G. Aad *et al.*, "Constraints on the off-shell Higgs boson signal strength in the high-mass ZZ and WW final states with the ATLAS detector," *Eur. Phys. J.* **C75** (2015) no. 7, 335, `arXiv:1503.01060 [hep-ex]`.

[49] **ATLAS** Collaboration, M. Aaboud *et al.*, "Measurement of the Higgs boson mass in the $H \to ZZ^* \to 4\ell$ and $H \to \gamma\gamma$ channels with $\sqrt{s} = 13$ TeV pp collisions using the ATLAS detector," *Phys. Lett.* **B784** (2018) 345–366, `arXiv:1806.00242 [hep-ex]`.

[50] **ATLAS** Collaboration, M. Aaboud *et al.*, "Constraints on off-shell Higgs boson production and the Higgs boson total width in $ZZ \to 4\ell$ and $ZZ \to 2\ell 2\nu$ final states with the ATLAS

detector," *Phys. Lett.* **B786** (2018) 223–244, `arXiv:1808.01191 [hep-ex]`.

[51] J. M. Campbell, R. K. Ellis, and C. Williams, "Bounding the Higgs width at the LHC using full analytic results for $gg \to e^-e^+\mu^-\mu^+$," *JHEP* **04** (2014) 060, `arXiv:1311.3589 [hep-ph]`.

[52] J. M. Campbell, R. K. Ellis, and C. Williams, "Gluon-Gluon Contributions to W+ W- Production and Higgs Interference Effects," *JHEP* **10** (2011) 005, `arXiv:1107.5569 [hep-ph]`.

[53] J. M. Campbell, R. K. Ellis, and C. Williams, "Bounding the Higgs Width at the LHC," *PoS* **LL2014** (2014) 008, `arXiv:1408.1723 [hep-ph]`.

[54] W. Buchmuller and D. Wyler, "Effective Lagrangian Analysis of New Interactions and Flavor Conservation," *Nucl. Phys.* **B268** (1986) 621–653.

[55] B. Grzadkowski, M. Iskrzynski, M. Misiak, and J. Rosiek, "Dimension-Six Terms in the Standard Model Lagrangian," *JHEP* **10** (2010) 085, `arXiv:1008.4884 [hep-ph]`.

[56] T. Barklow, K. Fujii, S. Jung, M. E. Peskin, and J. Tian, "Model-Independent Determination of the Triple Higgs Coupling at e+e- Colliders," *Phys. Rev. D* **97** (2018) no. 5, 053004, `arXiv:1708.09079 [hep-ph]`.

[57] J. Cohen, S. Bar-Shalom, and G. Eilam, "Contact Interactions in Higgs-Vector Boson Associated Production at the ILC," *Phys. Rev. D* **94** (2016) no. 3, 035030, `arXiv:1602.01698 [hep-ph]`.

[58] L. J. Dixon, "Calculating scattering amplitudes efficiently," in *QCD and beyond. Proceedings, Theoretical Advanced Study Institute in Elementary Particle Physics, TASI-95, Boulder, USA, June 4-30, 1995*, pp. 539–584. 1996. `arXiv:hep-ph/9601359 [hep-ph]`. `http://www-public.slac.stanford.edu/sciDoc/docMeta.aspx?slacPubNumber=SLAC-PUB-7106`.

[59] G. Passarino and M. J. G. Veltman, "One Loop Corrections for e+ e- Annihilation Into mu+ mu- in the Weinberg Model," *Nucl. Phys.* **B160** (1979) 151–207.

[60] X. Chen, G. Li, and X. Wan, "Probe CP violation in $H \to \gamma Z$ through forward-backward asymmetry," *Phys. Rev.* **D96** (2017) no. 5, 055023, `arXiv:1705.01254 [hep-ph]`.

[61] T. Binoth, N. Kauer, and P. Mertsch, "Gluon-induced QCD corrections to pp$\to$ ZZ $\to$ l anti-l l-prime anti-l-prime," in *Proceedings, 16th International Workshop on Deep Inelastic Scattering and Related Subjects (DIS 2008): London, UK, April 7-11, 2008*, p. 142. 2008. `arXiv:0807.0024 [hep-ph]`.

[62] J. M. Campbell, R. K. Ellis, and W. T. Giele, "A Multi-Threaded Version of MCFM," *Eur. Phys. J.* **C75** (2015) no. 6, 246, `arXiv:1503.06182 [physics.comp-ph]`.

[63] R. Boughezal, J. M. Campbell, R. K. Ellis, C. Focke, W. Giele, X. Liu, F. Petriello, and C. Williams, "Color singlet production at NNLO in MCFM," *Eur. Phys. J.* **C77** (2017) no. 1, 7, `arXiv:1605.08011 [hep-ph]`.

[64] A. D. Martin, W. J. Stirling, R. S. Thorne, and G. Watt, "Parton distributions for the LHC," *Eur. Phys. J.* **C63** (2009) 189–285, `arXiv:0901.0002 [hep-ph]`.

[65] **CMS Collaboration** Collaboration, C. Collaboration, "Properties of the Higgs-like boson in the decay H to ZZ to 4l in pp collisions at sqrt s =7 and 8 TeV," Tech. Rep. CMS-PAS-HIG-13-002, CERN, Geneva, 2013. `http://cds.cern.ch/record/1523767`.

[66] F. Caola, K. Melnikov, R. Rontsch, and L. Tancredi, "QCD corrections to ZZ production in gluon fusion at the LHC," *Phys. Rev.* **D92** (2015) no. 9, 094028, `arXiv:1509.06734 [hep-ph]`.

[67] K. Melnikov and M. Dowling, "Production of two Z-bosons in gluon fusion in the heavy top quark approximation," *Phys. Lett.* **B744** (2015) 43–47, `arXiv:1503.01274 [hep-ph]`.

[68] J. M. Campbell, R. K. Ellis, M. Czakon, and S. Kirchner, "Two loop correction to interference in $gg \to ZZ$," *JHEP* **08** (2016) 011, `arXiv:1605.01380 [hep-ph]`.

[69] F. Caola, M. Dowling, K. Melnikov, R. Rontsch, and L. Tancredi, "QCD corrections to vector boson pair production in gluon fusion including interference effects with off-shell Higgs at the LHC," *JHEP* **07** (2016) 087, `arXiv:1605.04610 [hep-ph]`.

[70] **CMS Collaboration** Collaboration, C. Collaboration, "Measurements of properties of the Higgs boson in the four-lepton final state in proton-proton collisions at $\sqrt{s} = 13$ TeV," Tech. Rep. CMS-PAS-HIG-19-001, CERN, Geneva, 2019. `http://cds.cern.ch/record/2668684`.